Computers and Fluids 303 (2025) 106875

Contents lists available at ScienceDirect

Computers and Fluids

journal homepage: www.elsevier.com/locate/compfluid

Turbulence model uncertainty estimation via Monte Carlo perturbation of the Reynolds Stress Tensor☆

Giulio Gori

Department of Aerospace Science and Technology, Politecnico di Milano, Via La Masa, 34, Milano, 20156, Italy

ARTICLE INFO

Keywords:
Uncertainty quantification
Eigenspace Perturbation Method
RANS
Turbulence uncertainty

ABSTRACT

We propose to rely on a flat Dirichlet distribution to sample the eigenvalues of the Reynolds Stress Tensor in RANS simulations. The goal is to forward propagate the uncertainty inherent the structure of the turbulence closure to targeted QoIs. The flat Dirichlet distribution is defined over the 2-dimensional simplex delimiting the Reynolds Stress Tensor realizability conditions. This ensures the tensor positive-definiteness and serves the uncertainty forward propagation by means of diverse techniques e.g., Monte Carlo or Polynomial Chaos Expansions. Simulations are performed using a modified version of the open-source SU2 suite. Results are obtained for two reference test cases. Namely, the subsonic air flow over a backward facing step and the NACA0012 airfoil operating in subsonic conditions and with a variable angle of attack.

1. Introduction

Reynolds-averaged Navier–Stokes (RANS) simulations with turbulence closure models are still the standard in industrial flow simulations since they offer an affordable trade-off between accuracy and computational cost. Unfortunately, the strong inherent assumptions underlying turbulence closures employed in Computational Fluid Dynamics (CFD) are known to limit the credibility of numerical predictions [1]. Literature is teemed with works devoted to improving the modeling of turbulent flows. These efforts relentlessly develop new modeling strategies based on theoretical, heuristic, or data-driven, approaches. Nonetheless, the quest of obtaining a reliable turbulence model of general validity is still out of reach. Moreover, the complexity of the task is increased due to a nontrivial understanding of the turbulence modeling error propagation in RANS, which was recently investigated in [2–4]. The direct quantification of the uncertainty associated to turbulence closures is demanding, if not intractable, requiring the community to devote efforts to the development of formal and practical Uncertainty Quantification (UQ) techniques [5].

In this work, we take advantage of the Eigenspace Perturbation Method (EPM) [6,7], also referred to as Eigenspace Perturbation Framework [8]. The EPM is designed to obtain reasonable and informed uncertainty estimates of selected Quantity of Interest (QOIs) of the turbulent flow. In its standard implementation [9], the EPM entails the realization of 5 different CFD simulations of the problem under investigation. Each realization corresponds to a specific perturbation of the Reynolds Stress Tensor (RST). Ultimately, the five different predictions provide an estimate of the uncertainty associated to the structural deficiency of the turbulence closure. We stress the deliberate use of the word estimation, rather than quantification, since the method provides only uncertainty estimates rather than rigorous and provable bounds on the prediction. Lately, the methodology became quite popular and has been applied to canonical problems in turbulent flows, with extension to Large Eddy Simulations [10]. Investigations were also devoted to understanding the physical plausibility of the standard EPM approach, see [11]. Recently, critiques has been moved concerning the consistency of the perturbed RST stemming from the common EPM implementation [8], showing that the combination of eigenvector perturbation and moderation factor (typically employed to improve the stability of the solver) may lead to nonphysical Reynolds stress dynamics. According to this latter analysis, in Ref. [8] the Authors derive a set of necessary physics-based constraints that need to be fulfilled to overcome the issue. The EPM was also exploited for different purposes. For instance, it has been coupled with data-driven algorithms [12] and employed to devise optimization strategies accounting for the credibility of the CFD model e.g., Refs. [13–17].

The quest of improving the EPM is a prolific research ground. Researchers investigate strategies to generate random realizations of the RST, see [18]. In Ref. [12], the authors propose a mapping between a pair of natural to a pair of physical coordinates. On top of this work, in Ref. [19,20] the authors present a further extension including the use of Euler angles for parameterizing the perturbations of the Reynolds

☆ This article is part of a Special issue entitled: 'ICCFD12-2024' published in Computers and Fluids.

E-mail address: giulio.gori@polimi.it.

https://doi.org/10.1016/j.compfluid.2025.106875
Received 18 March 2025; Received in revised form 23 August 2025; Accepted 9 October 2025
Available online 13 October 2025

stress eigenvectors, proposing a random matrix approach which directly samples a maximum entropy distribution defined on the set of positive semidefinite matrices. In Refs. [21,22], it is instead proposed to employ unit-quaternion in place of the Euler's angles and the EPM is applied in the context of machine learning assisted RANS and UQ. A recent paper from Jewell et al. [23] presents an innovative approach for modeling and quantifying model-form uncertainty based on the EPM. Namely, they present a computationally tractable bipartite algorithm that complements a hyperparameterized probabilistic representation of the turbulence model, based on a stochastic RST through EPM, with a nonparametric probabilistic method for nonlinear structural dynamics. Specifically to the RST, the Authors handle UQ by generating a family of turbulence models thanks to hyperparameterized perturbations to the anisotropic part. Perturbations include modifications of the eigenvalues, eigenvectors, and also the turbulent kinetic energy, and depend on random samples of auxiliary variables which are accepted only if within certain intervals.

In this paper, we focus on the eigenvalues perturbations only. The goal is to forward propagate the uncertainty related to the RST spectrum to the targeted QoIs, for instance using a plain Monte Carlo approach. In general, parametrization strategies are possibly subject to shortcomings. For instance, the mapping employed in [12] does not generally guarantee the realizability of the perturbed RST, admittedly requiring the implementation of an ad hoc clipping strategy to handle any out-of-bound perturbation. In practice, the authors apply a Gaussian perturbation to the baseline model and the corrupted samples, that is, the samples that are mapped outside the realizability space, are forcefully repositioned on the boundary. As a consequence of this clipping, the resulting prior may become non-Gaussian and with non zero-mean. This is particularly critical if the baseline Reynolds stresses are located near the realizability boundaries. Although the approach allows to estimate and control the percentage of out-of-bound points, admittedly the machinery relies on ad hoc modeling choices. Similar issues are found related to some of the parametrization strategies mentioned earlier.

We propose to rely on a flat Dirichlet distribution on a 2-dimensional simplex to directly sample the barycentric coordinates of the RST eigenvalues. This type of parametrization prevents the shortcomings described above. Namely, sampling the eigenvalues from a Dirichlet distribution ensures positive definite realizations of the RST without the need of clipping. Moreover, the definition of a Dirichlet distribution provides a means to formally characterize the uncertainty affecting the RST eigenvalues. By changing the concentration parameters of the distribution, the modeler can encode prior knowledge in an arbitrary manner. We stress that the aim of this work is not to prove the general superiority of the proposed parametrization w.r.t. former ones, but rather to add a new way of handling the UQ analysis that may come handy in some cases. At the price of an increased computational cost, sampling from a Dirichlet distribution is surely a more flexible approach that allows full control over the eigenvalue perturbations. Its practical usage is quite straightforward since it almost maintains the standard implementation of the EPM, with just minor modifications required, in existing computer codes e.g., SU2. The characterization of uncertainty based on the Dirichlet distribution may also easily serve the forward propagation of the uncertainty by means of advanced UQ techniques e.g., Polynomial Chaos, for which we report an example.

In this work, CFD simulations are performed using the open-source SU2 suite [24,25], in particular the EQUiPS module enabling EPM capabilities [26]. Note that the EQUiPS module implements the standard EPM from [9], and it includes some clipping operations on the turbulent kinetic energy production term. To achieve our goals i.e., to accommodate the injection of arbitrary perturbations stemming from the sampling of the Dirichlet distribution, the source code was slightly modified.

This paper develops according to the following structure. Section 2 briefly recalls the fundamentals of the EPM are summarized in Section 2. There, we also present the sampling strategy applied to obtain random realizations of the RST. Results are reported in Section 3 and concern two reference tests. Namely, the subsonic flow of air over a backward facing step and the subsonic flow of air over a NACA0012 airfoil at a variable angle of attack. Conclusions are exposed in Section 4.

2. Methodology

We describe the fluid model namely, the incompressible RANS model, and the UQ framework based on the EPM.

2.1. The RANS model

The RANS CFD model is a set of partial differential equations obtained from the time-averaged decomposition of the viscous incompressible Navier–Stokes fluid model. According to the Reynolds averaging process, and retaining the notation from the popular book of Pope [27], the instantaneous local quantities (upper case) are decomposed into a time average (identified with the angle bracket) plus a fluctuation (lower case). For instance, the local field velocity reads

$$\mathbf{U} = \langle \mathbf{U} \rangle + \mathbf{u}, \tag{1}$$

where the vectors belong to the a three dimensional domain and the indices i, j, k, identify the different coordinates. Ultimately, the incompressible RANS model consists of the Reynolds equations

$$\frac{\partial \langle \mathbf{U} \rangle}{\partial t} + \langle \mathbf{U} \rangle \cdot \nabla \langle \mathbf{U} \rangle = \nu \nabla^2 \langle \mathbf{U} \rangle - \nabla \cdot \langle \mathbf{u} \otimes \mathbf{u} \rangle - \frac{1}{\rho} \nabla \langle p \rangle, \tag{2}$$

plus the continuity equation. In the above expression, ρ is the constant fluid density whereas ν is the kinematic viscosity. The term $\langle \mathbf{u} \otimes \mathbf{u} \rangle$ is a byproduct of the Reynolds averaging operation and it is due to the decomposition of the non-linear convective term included in the Navier–Stokes model. This encodes the covariance of the velocity fluctuations and goes under the name of the Reynolds Stress Tensor, here already abbreviated using RST. The RST plays a crucial role in modeling the behavior of the mean flow. Its physical interpretation is generally related to apparent stresses due to momentum transfer caused by velocity fluctuations, the reader is referred to [27] for a deeper insight.

From the discussion above, it is evident that the RANS model requires a closure for the components of the RST. In the past decades, many different turbulence models were proposed. Among the most popular ones, we surely find those based on the Boussinesq approximation, which relates the turbulent stress tensor to the mean velocity gradients. In the following, our goal is to model the RST by directly sampling its components based on random perturbations of the eigenspace of the baseline tensor computed by means of a standard turbulence closure.

2.2. The UQ framework

The EPM [6,7] consists in applying perturbations of finite amplitude to the eigenspace of the RST during the CFD iterations. The formal aspect of the methodology are well established and detailed in a number of reference papers [6–9,11,12,28]. Hereinafter, we briefly recall the fundamental aspects.

The physical admissibility of the RST requires it to be positive semidefinite, and this leads to the specification of the set of realizability conditions [29,30]

$$\langle u_i u_i \rangle \geq 0, \quad \langle u_i u_i \rangle + \langle u_j u_j \rangle \geq \left| 2 \langle u_i u_j \rangle \right|, \quad \det\left(\langle u_i u_j \rangle \right) \geq 0. \tag{3}$$

with $i, j = \{1, 2, 3\}$. Since the RST can be decomposed into an anisotropy and a deviatoric part

$$\langle u_i u_j \rangle = 2k_t \left(v_{ik} \Lambda_{kl} v_{jl} + \frac{\delta_{ij}}{3} \right), \tag{4}$$

it follows that realizability conditions apply also to the anisotropy tensor. In the above expression, the anisotropy part is expressed in its

spectral form (v_{ik} and v_{jl} are the left and the right eigenvectors, Λ_{kl} a diagonal matrix containing the eigenvalues λ_i).

During the CFD iterations, the EPM injects perturbations of finite amplitude to the eigenspace of the RST provided by a baseline turbulence closure. Under the condition of that the realizability conditions Eqs. (3) are fulfilled, any quantity in Eq. (4) may be perturbed

$$\left\langle u_i u_j \right\rangle^* = 2k_t^* \left(v_{ik}^* \Lambda_{kl}^* v_{jl}^* + \frac{\delta_{ij}}{3} \right), \tag{5}$$

with the superscript * indicating a perturbed entity. According to this approach, the whole realizability space might be explored to estimate the structural uncertainty inherent in the turbulence closure. To simulate perturbed flows, we take advantage of the open-source SU2 suite [24,25]. SU2 is equipped with EPM capabilities [26] that implement the approach described in [9]. The perturbation of the eigenvalues is modulated by an under-relaxation factor described in [18] (In this work, we employ a default value of 0.1). In general, uniform spatial perturbations apply to the eigenvalues Λ_{kl}^* and eigenvectors v_{ik}^*, whereas perturbations of the k_t are not considered.

In summary, in its standard implementation, the EPM entails the execution of five simulations additional to the baseline one (unperturbed turbulence closure), each associated with a specific realizations of the RST. Namely, eigenvalue perturbations seek three extremal states of turbulent componentiality (labeled $1C$, $2C$, and $3C$) combined with extremal states associated with the production of turbulent kinetic energy ($\mathcal{P}^{max}$ and $\mathcal{P}^{min}$). The $1C$, $2C$, and $3C$ can be visualized as the vertexes of a triangle, see Fig. 1. Because of the realizability conditions, the RST eigenvalues expressed in barycentric coordinates must lie within the area of this triangle. In practice, $\mathbf{x}_{3C}$ corresponds to isotropic turbulence componentiality and is invariant to the perturbation of the eigenvectors. Hereinafter, we will adopt the following labels $\mathcal{P}_{1C}^{max}$ (PA), $\mathcal{P}_{2C}^{max}$ (PB), $3C$ (PC), $\mathcal{P}_{1C}^{min}$ (PD), $\mathcal{P}_{2C}^{min}$ (PE), and (BS) to indicate the baseline model. In the standard EPM, the turbulent uncertainty estimates of a selected performance p are then obtained by considering the maximum prediction dispersion resulting from the five EPM solutions plus the BS according to

$$\Delta_p^{\mathrm{EPM}} = \max(p^{\mathrm{BS}}, p^{\mathrm{PA}}, p^{\mathrm{PB}}, p^{\mathrm{PC}}, p^{\mathrm{PD}}, p^{\mathrm{PE}}) - \min(p^{\mathrm{BS}}, p^{\mathrm{PA}}, p^{\mathrm{PB}}, p^{\mathrm{PC}}, p^{\mathrm{PD}}, p^{\mathrm{PE}}), \tag{6}$$

which provides an estimation about the dispersion of RANS prediction due to the epistemic uncertainty inherent in the turbulence closure. In the following, we neglect PD and PE to reduce the computational burden and, most importantly, to avoid the effect of the eigenvector perturbation combined with the under-relaxation factor exposed in [8]. Namely, according to standard practice, in the SU2 implementation the eigenvalues perturbation is modulated by an under-relaxation factor to improve the stability of CFD simulations. In particular, the referenced paper sheds light on nontrivial implications inherent the use of such moderation factor which may lead to a loss of physical consistency. To overcome the issue, Matha et al. [8] establish additional physics-based constraints that the EPM procedure must fulfill. The CFD solver SU2 lacks these additional constraints, therefore eigenvector perturbations are here neglected, with a significant saving of computational resources. Besides, eigenvector perturbations build on top of eigenvalue perturbations for both the standard parametrization (EPM with extremal perturbations) and the proposed one (Dirichlet), adding no value to the comparison among the two. Although naive approaches may be implemented, formalization of this step is left to future investigations.

The methodology described so far provides a clever way to provide estimates of the prediction uncertainty. To implement the our UQ framework, we propose to sample the RST eigenspace by relying on a flat Dirichlet distribution on a 2-dimensional simplex. Note that the choice of a flat distribution is arbitrary. Potentially, the user may manipulate it to obtain substantially different distributions over the realizability triangle and encode diverse prior knowledge. Here, we select a symmetric distribution with concentration parameter $\alpha = 1$, reading

$$\mathcal{P}_{\mathrm{Dir}}(\boldsymbol{w};\boldsymbol{\alpha}) \sim \frac{1}{\mathrm{B}(\boldsymbol{\alpha})} \prod_{k=1}^{3} w_k^{\alpha_k - 1}, \qquad \mathrm{B}(\boldsymbol{\alpha}) = \frac{\prod_{k=1}^{3} \Gamma(\alpha_k)}{\Gamma\left(\sum_{k=1}^{3} \alpha_k\right)}, \qquad \boldsymbol{\alpha} = (1,1,1), \tag{7}$$

being the normalizing constant $\mathrm{B}(\boldsymbol{\alpha})$ a multivariate beta function expressed in terms of the gamma function Γ. Each of the Dirichlet samples ($\boldsymbol{w}_i$) does not specify the eigenvalues of the anisotropy tensor, but rather defines the weights of the eigenvalue in the barycentric map with vertices $\mathbf{x}_{1C} = (0.0, 0.0)$, $\mathbf{x}_{2C} = (1.0, 0.0)$, and $\mathbf{x}_{3C} = \left(0.5, \sqrt{3}/2\right)$. By construction, each sample $\boldsymbol{w}_i$ satisfies the constraint $\sum_{d=0}^{3} w_{i,d} = 1$. Therefore, the following mapping holds

$$x_i = w_{i,1} x_{1C} + w_{i,2} x_{2C} + w_{i,3} x_{3C}, \qquad y_i = w_{i,1} y_{1C} + w_{i,2} y_{2C} + w_{i,3} y_{3C}. \tag{8}$$

This convex combination of the vertexes $1C$-$2C$-$3C$ allows to generate random points uniformly distributed within the RST realizability space, see Fig. 1(a). Ultimately, the approach can be employed to forward propagate the structural uncertainty related to the turbulence closure to any QoIs, for instance using a plain Monte Carlo approach. We employ a flat Dirichlet distribution, but the selection of nonsymmetric components of the concentration vector $\boldsymbol{\alpha}$, would allow to control the positioning of the bulk of the probability density anywhere within the realizability space, providing a means to promote or penalize the sampling in specific regions.

Additionally, characterizing the uncertainty is fundamental for the use of efficient UQ techniques e.g., the construction of Polynomial Chaos-based surrogates. The Gauss–Laguerre quadrature rule can be applied to sample the simplex at the root of Laguerre polynomials which, according to the Askey scheme, are associated with the Gamma distributions used to build the Dirichlet one, see Fig. 1(b). In this way, it is possible to build the full-tensor product and numerically integrate the orthogonal projection of the random response to compute the expansion coefficients.

In the following, we produce Monte Carlo estimates of the statistics of diverse QoIs for two application cases i.e., a subsonic stream over a backward facing step and a NACA 0012 airfoil at different angles of attack. For the second test case, we build Polynomial Chaos surrogates, assessing their suitability in handling the proposed setting.

3. Results

3.1. Backward facing step (BF-STEP)

This test corresponds to the 2DBFS validation case for turbulence models provided by the NASA TMR (Turbulence Modeling Resource) [31,32]. The very same problem is included in the ERCOFTAC Database (Classic Collection) #30, and we consider a null inclination of the upper wall. This is a widely-tested configuration [33–36]. The NASA TMR provides a series of 2D structured grids of different quality and resolution. Here, we employ the quite coarse grid 65x65-25x65-97x113-33x113. We do acknowledge that this grid is not sufficient to represent the full physics of the backward facing step. Indeed, the dissipation caused by the coarse resolution damps the flow unsteady features which typically make the convergence to a time accurate solution difficult to achieve (see the SSTm or the SSTVm Model Results from NASA TMR). With this grid, CFD simulations easily converge to a steady solution. In our case, the grid choice is driven by the computational cost of the Monte Carlo analysis (based on 10'000 samples for this case). Despite the rough approach, predictions are in line with experimental measurements and with benchmark comparison against data provided on the NASA TMR repository.

The Reynolds number is approximately 36,000 based on step height $H = 0.0127$ m. The total conditions applied at the inlet boundary are a

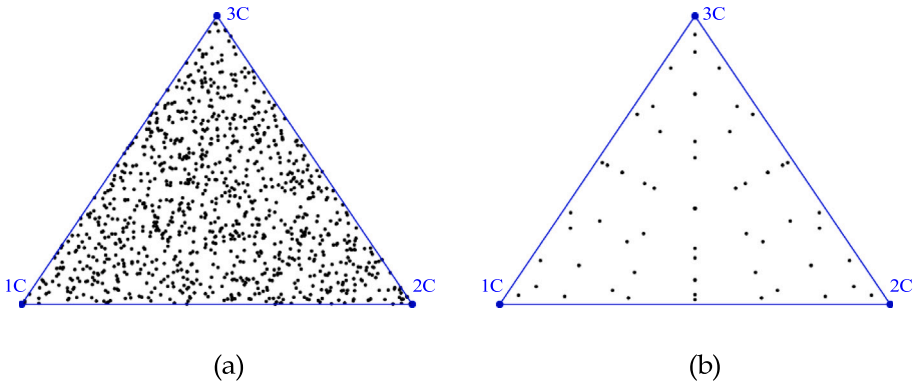

Fig. 1. (a) Uniform random sampling over the barycentric map of the eigenvalues in the Euclidean space. (b) Full-tensor Gauss–Laguerre quadrature sampling.

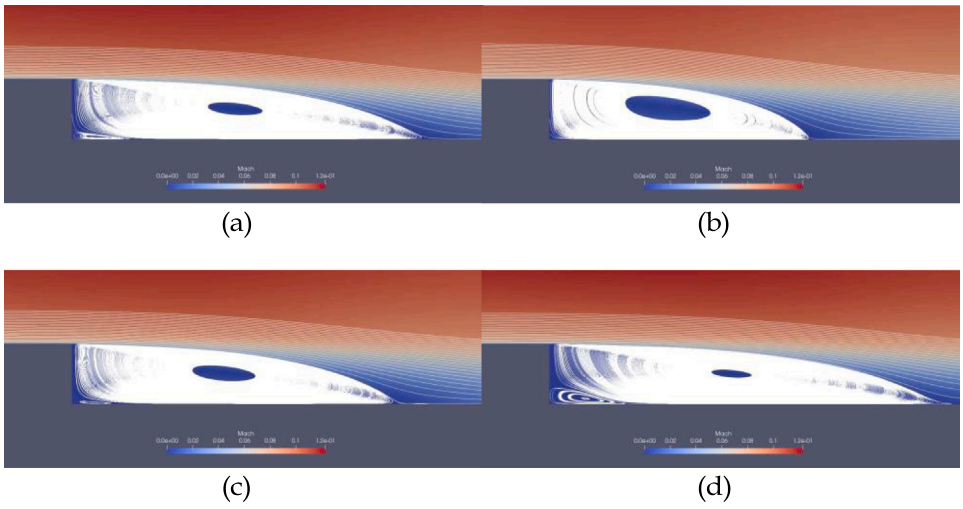

Fig. 2. BF-STEP Mach field and streamlines. (a) BS. (b) PA. (c) PB. (d) PC.

total pressure $p_0 = 100171.440$ Pa and a total temperature $T_0 = 297.359$ K, whereas at the outlet a static pressure value of $p = 99300$ Pa is used. At these conditions, the Mach number upstream the step is about 0.128, as indicated for this test case. Considering the BS turbulence model i.e., the Menter's Shear Stress Transport (SST) closure [37], the length of the inflow segment is large enough to promote the full development of the boundary layer ahead of the step. A no slip wall condition applies on the remaining boundaries.

A Monotone Upstream-centered Schemes for Conservation Laws (MUSCL) approach with gradient limitation based on the popular upwind Roe scheme was employed [38]. Gradient reconstruction was carried out using the Green–Gauss approach. Convergence was assessed by requiring a reduction of the density residual of 10 orders of magnitude. A maximum number of iteration is set at 40,000, but this limit is never reached for all the simulations considered in this Section.

Figs. 2 show the Mach fields and the fields streamlines as predicted from the BS, PA, PB, and PC models, respectively. Clearly, the different perturbations applied to the RANS turbulence closure lead to the development of diverse solutions. In particular, it is evident that the shape of the recirculation bubble is largely influenced by the applied perturbation. The length of the recirculation bubble is indeed one of the QoIs targeted by the Monte Carlo analysis.

We first present the UQ analysis concerning the pressure coefficient (C_p) and the skin friction coefficient (C_f) along the lower domain wall i.e., the portion of the lower boundary originating past the step, being the position of the step at $x/H = 0$. For both quantities, we report the Δ^{EPM} indicator from the standard EPM (considering only BS, PA, PB, and, PC) and the $2\sigma_{\text{std}}$ envelope resulting from the Monte Carlo analysis. The first one is reported as a red shaded area whereas the second is the gray shaded area. The black continuous line is the average of the Monte Carlo analysis, whilst the green line is the prediction from the BS model. The dots indicate instead the experimental measure.

Concerning the pressure coefficient, Fig. 3(a) shows that numerical predictions fairly approach the experimental trend. Note that, according to common practice, the C_p values are shifted so that $C_p(x/H \approx 40) \approx 0$. Overall, the BS predictions (green) underestimates the C_p value, with the largest discrepancy found at $x/H \approx 8$. Results are in line with the benchmark data provided on the NASA TMR repository. In most of the domain, the experimental data are found outside both the Δ^{EPM} and the $2\sigma_{\text{std}}$ envelopes, indicating that the uncertainty inherent the sole distribution of energy among the eigenmodes of the RST cannot explain the discrepancy in the numerics-experiment comparison. The two uncertainty envelopes are comparable in terms of width and covered region.

Similar considerations apply to the skin friction coefficient which is reported in Fig. 3(b). The BS prediction fairly matches the experimental data, except for the first portion of the domain where the CFD model provides lower outputs. The $2\sigma_{\text{std}}$ and Δ^{EPM} envelopes are again comparable, the latter being generally a bit larger.

Given the number of realizations available, we estimate the probability distribution of the targeted QoIs at local stations along the lower wall, using a Gaussian kernel. The results obtained are plotted in Fig. 4 for both the pressure and the skin friction coefficients. At each station, the local probability distribution has been scaled in order to set the peak of relative likelihood to 1. The scaling was needed to set a comparable colormap and to identify the locus of most likely values

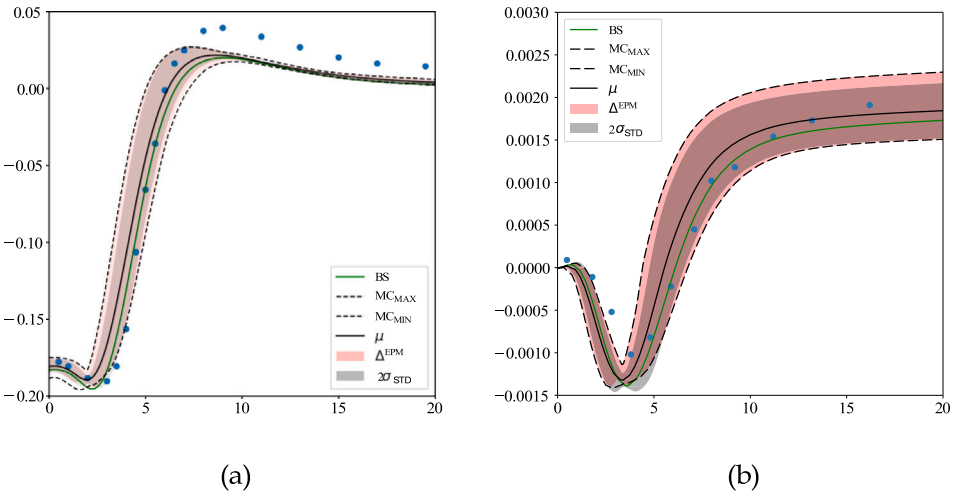

Fig. 3. BF-STEP. (a) Pressure coefficient C_p over the lower wall. (b) Skin friction coefficient C_f over the lower wall.

w.r.t. the position along the lower wall. Although the standard EPM just provides reasonable and informed uncertainty estimates (rather than rigorous and provable bounds), the Δ^{EPM} envelope largely contains the bulk of the probability distribution for all the lower wall length. Of particular interest is the $x/H \approx 3$ station in Fig. 4(b), at which we see that the most likely predicted C_f is found outside Δ^{EPM}. This region corresponds basically to the portion of the lower wall subject to a reverted flow positioned below the core of the primary re-circulation bubble. Here, the lower bound of the Δ^{EPM} is indeed determined by the BS prediction, see Fig. 3(b). The most probable prediction stemming from the UQ Monte Carlo analysis is even lower than the BS solution, which is anyway well included within the $2\sigma_{\text{std}}$. Nonetheless, we stress that the probability density function is estimated considering a flat Dirichlet distribution over the whole realizability space of the RST. This encodes complete ignorance concerning the eigenvector coordinates except just the knowledge of the realizability limits. In this approach, we include many realizable yet not plausible perturbations of the RST [11]. Clearly, a different specification of the Dirichlet distribution e.g., selecting non symmetric components of the concentration parameters vector $\boldsymbol{\alpha}$, would allow to force the bulk of the Reynolds stresses probability density anywhere within the realizability boundaries. By playing with the concentration parameters, the user would also be able to penalize the exploration of the region of the realizability triangle which are likely to be associated to not plausible Reynolds stresses.

For this test case, the standard EPM provides a good approximation of the Monte Carlo envelope stemming from the sole perturbation of the eigenvalues. The Δ^{EPM} reasonably approximates the $2\sigma_{\text{std}}$ envelope, surely including the bulk of the probability density. Nonetheless, we remind that in our setting we are not perturbing the turbulent kinetic energy k_t or the eigenvectors of the anisotropy tensor, see Eq. (4). Therefore, the whole discussion should be revised in case these latter perturbations are also taken into account, also in view of the implications exposed in [8].

We focus now on the statistics of the flow reattachment point downstream the step. The reattachment point is identified from the CFD solution by finding the mesh nodes along the lower wall over which the skin friction coefficient changes its sign. Fig. 5 reports the distribution of predicted reattachment points as reconstructed from the 10'000 Monte Carlo realizations using kernel density estimation. In particular, the sample set is partitioned into 10 complementary sub sets of 1'000 samples each and the distribution is reconstructed for an increasing size of the Monte Carlo sample set, to provide a rough convergence analysis. The 10 different distributions are reported in a gray scale, being the darkest the one relative to the full Monte Carlo sample set, and shows almost overlapping curves. The reattachment point predictions are distributed normally around $x/H \approx 5.6$. In green, we report also the baseline prediction, which is found further downstream, whereas in blue we report the experimental measure from [31], complemented by the provided $2\sigma_{\text{std}}$ envelope. The BS prediction is fairly close to the experiment, surely well included within its $2\sigma_{\text{std}}$ envelope. The UQ analysis of the turbulence closure provides a quite large uncertainty range, with the bulk of the probability density displaced towards an early prediction of the flow reattachment point.

3.2. NACA0012 airfoil (AIRFOIL)

The reference test case corresponds to the 2DN00 test case provided by the NASA TMR (Turbulence Modeling Resource) [31,32]. The UQ analysis targets the airfoil aerodynamic coefficients namely *lift* (c_l), *drag* (c_d), *efficiency* ($EF = c_l/c_d$) and *pitching moment* (c_m). The computational domain is discretized using the 449×129 FAMILY I grid from the NASA TMR repository [31,32]. The mesh represents a reasonable trade-off between flow resolution and computational burden [39]. Rigorously, a set of meshes should be constructed. Indeed, different grids are required to simulate the diverse flow configurations developing from every single RST realization i.e., for each EPM perturbation. Nevertheless, the computational burden would be unbearable and common practice it select a unique grid based on the BS model. Simulations are terminated if the c_l and the c_d coefficients remain within a $\epsilon \approx 10^{-6}$ tolerance range for a significant 100 of consecutive iterations or at the reaching of the maximum iteration number (20,000). In general, simulations converge well below 3000 iterations, and the maximum iteration limit is never reached, at least for the values of the angle of attack considered hereinafter.

Figs. 6 show the Mach fields and the fields streamlines as predicted from the BS, PA, PB, and PC models, respectively, obtained at $\alpha = 20°$. As expected, diverse solutions are obtained. As the airfoil is operating at a high angle of attack, the BS solution presents a partially separated region in the aft part, underestimating the onset of stall (experiments predict stall onset at about 17 °−18 °). Different EPM perturbations develop peculiar solutions. PA results into a fully attached flow, whereas PC increases the extent of the recirculation bubble developing in the aft portion of the airfoil. In general, these facts may be interpreted in view of the physical meaning of the extremal states of turbulence sought by the specific EPM perturbation. Nonetheless, to maintain the cost of the Monte Carlo analysis reasonable we rely on a coarse grid and on a loose CFD convergence criteria. Moreover, the clipping operation on the turbulent kinetic energy production term operated in the current SU2 implementation of the EPM appears to have relevant consequences

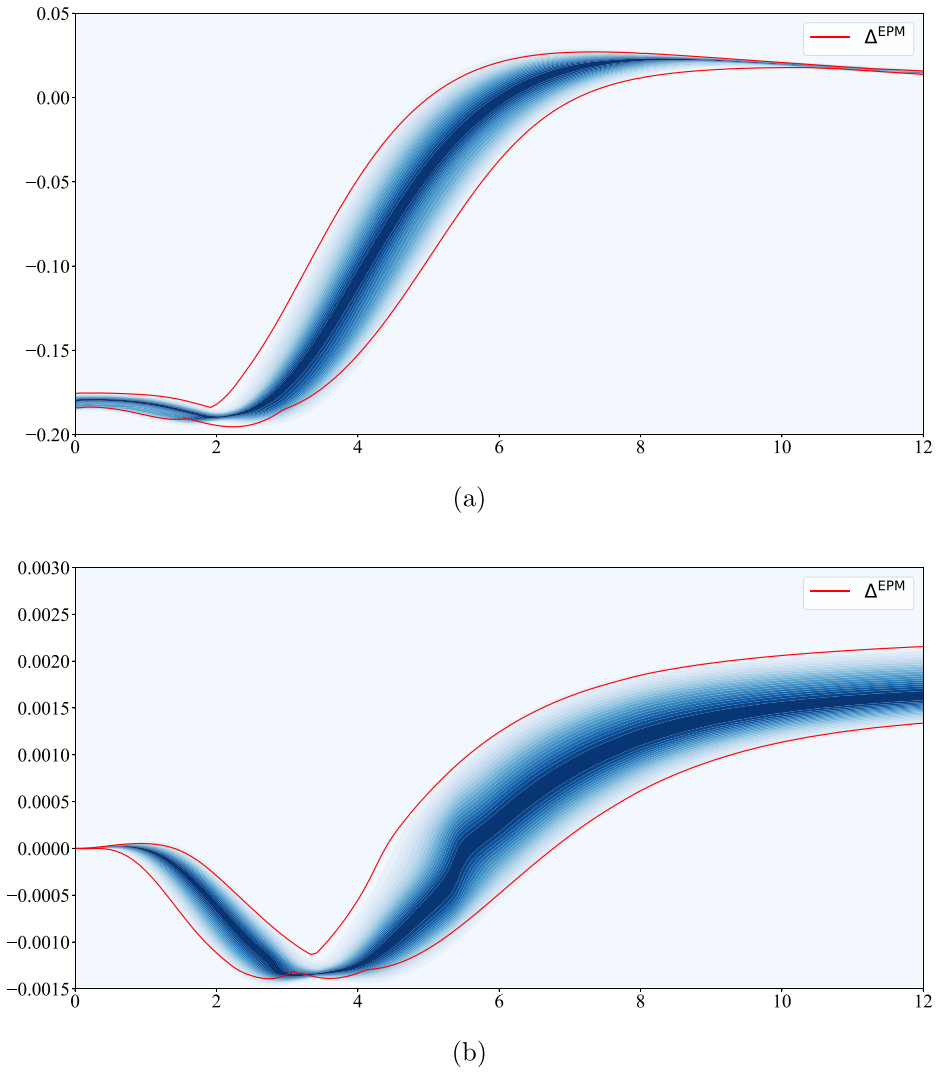

Fig. 4. BF-STEP. (a) Pressure coefficient C_p over the lower wall. (b) Skin friction coefficient C_f over the lower wall.

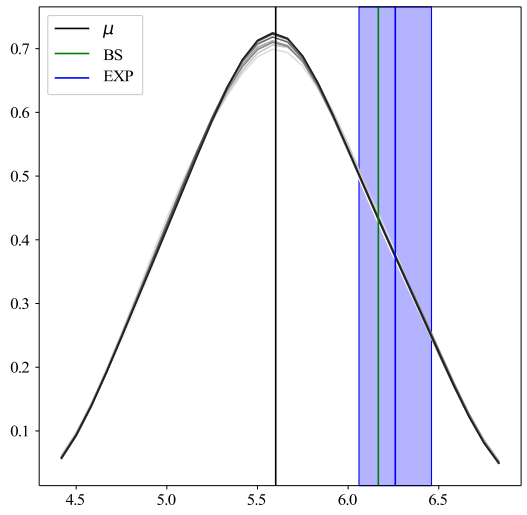

Fig. 5. BF-STEP. Monte Carlo analysis of the flow reattachment point prediction.

on the UQ analysis. For these reasons, we only focus on the investigation of the differences between the diverse UQ approaches in terms of predicted uncertainty estimates. Namely, we consider specific CFD models with fixed grid and numerical setting.

We perform a Monte Carlo analysis of airfoil performances in the interval $\alpha \in [0° - 20°]$ and considering 1000 realizations for each value of α, see Fig. 7. The plots report the mean of the Monte Carlo data set (μ) complemented by the $2\sigma_{\text{std}}$ envelope. Note that the data set has been cleansed from very few points that were associated to corrupted CFD simulations. These were identified as points outside the $5\sigma_{\text{std}}$ range and were at most 10 for $\alpha = 7°$, less than 5 for $\alpha = 9°, 10°$, 2 or even none for the remaining angles of attack). The envelope is very limited for the lift coefficient, as expected since we are mostly considering the linear portion of the c_l-α curve, becoming larger for α approaching the stall value. The other QoIs show a larger envelope, indicating a prominent uncertainty due to the turbulence closure. In terms of amplitude, the standard EPM min/max envelope is comparable to the $2\sigma_{\text{std}}$ envelope. Interestingly, the two envelopes maintain a comparable amplitude but, at large α, they do not overlap. It has to be stressed that the fact that the magnitude of the two envelopes is comparable is not of general validity, but rather a rough coincidence as shown in the following. Moreover, plotting the sole $2\sigma_{\text{std}}$ envelope does not provide an indication concerning the skewness of the distribution.

Since we rely on a Monte Carlo analysis, we reconstruct the full probability distribution of the variables via kernel density estimation. Fig. 8 reports the probability distributions associated to the four performances, for a value of $\alpha = 0°$, 6°, 12°, and 18° only. In the plot, we

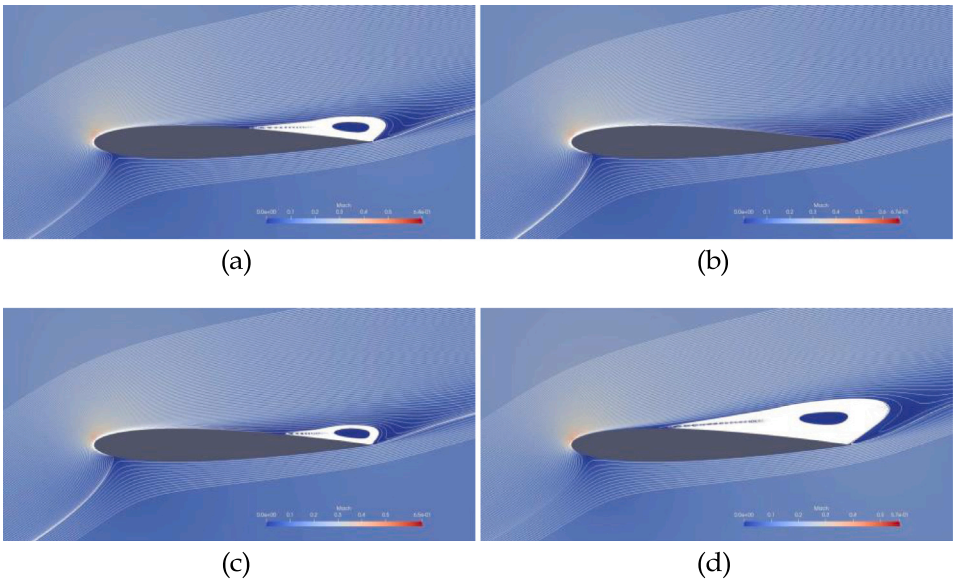

Fig. 6. AIRFOIL Mach field and streamlines. (a) BS. (b) PA. (c) PB. (d) PC.

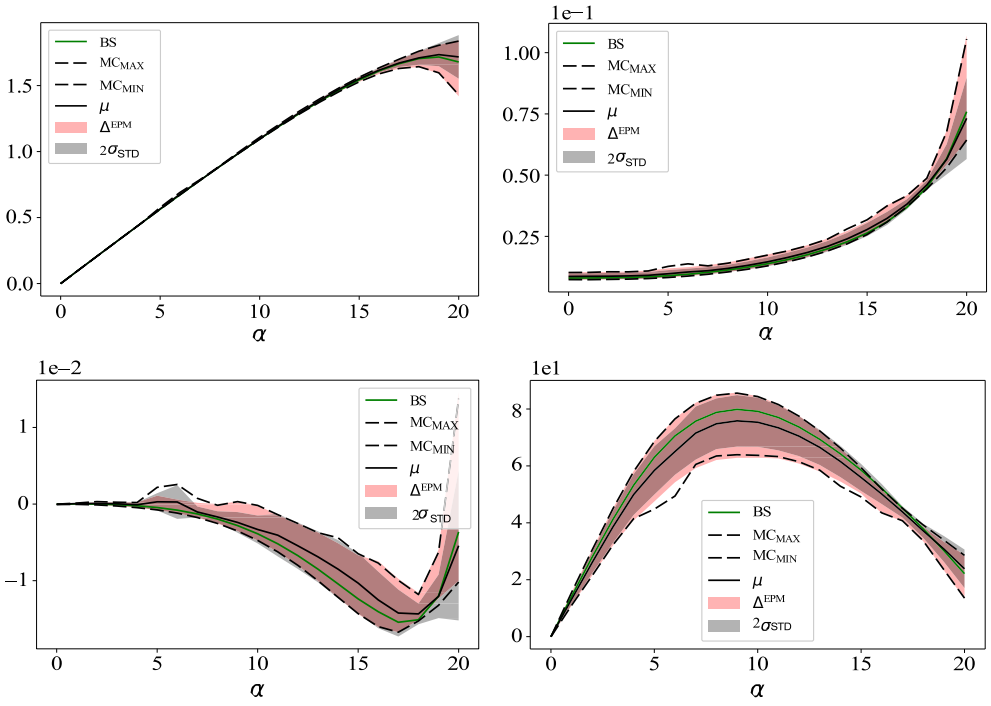

Fig. 7. AIRFOIL. Figures plot the mean and the 2σ envelope resulting from the Monte Carlo analysis of the targeted QoIs.

report the probability density as estimated for a data sets of increasing dimension, the smallest including 100 elements (white), the largest 1000 (black), underlying a convergence of the estimated curve w.r.t. the Monte Carlo samples. The densities are compared against the BS (blue vertical line) and the PA-PB-PC (red vertical lines) predictions. Although these latter do often include the bulk of the probability distribution, the extremal states are not representative of the effective uncertainty. This is clear from the plots relative to $\alpha = 6°$, for which we observe a multimodal distributions with points placed well outside the Δ^{EPM}. In fact, there is a considerable number of realizations which falls outside the Δ^{EPM}, for each of the four considered QoIs. This is of course an expected issue concerning the EPM. Indeed, it is widely known that, due to the nonlinearity of the fluid equations, the method provides uncertainty estimates rather than rigorous and provable bounds. Instead, the probability density associated to the QoIs for $\alpha = 18°$ (about the stall value) indicates that, in the considered setting, the standard EPM approach may be overly conservative since the extremal states of turbulence componentiality lead to quite unlikely predictions e.g., see the plot relative to c_l and c_m. This is not surprising either, because extremal states of turbulence componentiality are seldom in practical applications, if not even implausible. In fact, the standard implementation of the EPM was already proved to provide realizable but not plausible realizations of the RST, see [11].

The bottom line is, once again, that the sole indications provided by the EPM perturbations to the extremal states PA-PB-PC may be incomplete and insufficient to characterize the uncertainty stemming from the structure of the turbulence closure. Carefulness should be pledged in exploiting such information in aerospace applications e.g., design

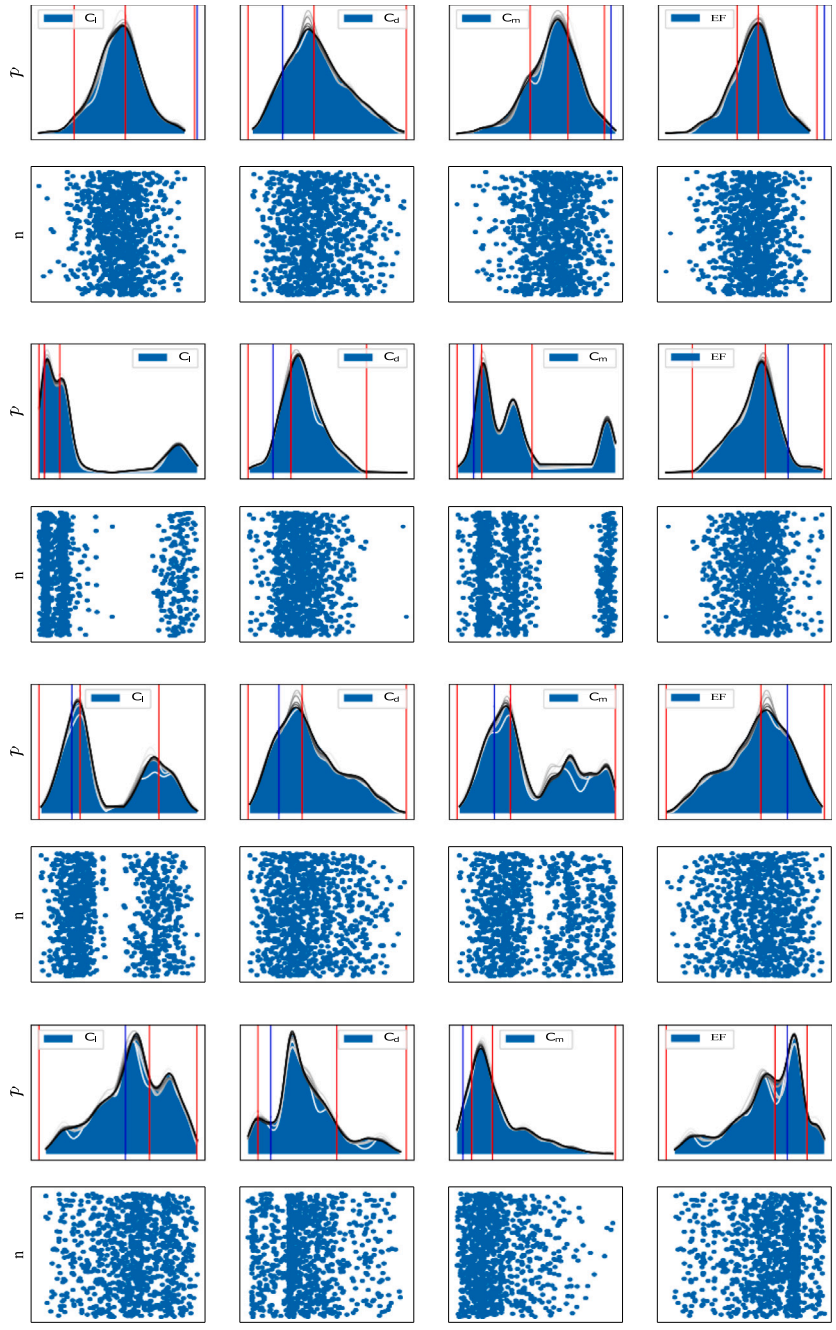

Fig. 8. AIRFOIL. Estimation of the probability density and scatter plot of the Monte Carlo realizations for the four QoIs ($\alpha = 0°$, $6°$, $12°$, and $18°$ from top to bottom).

optimization [15]. Nonetheless, the cost associated to a Monte Carlo analysis would be unbearable in practice, if not just for very simple cases, rendering worth the exploration of possible implementation of advanced uncertainty quantification techniques.

3.2.1. UQ via polynomial chaos expansion

As the cost of carrying out a full Monte Carlo analysis to forward propagate the epistemic uncertainty in turbulence closures based on the EPM approach would be computationally too demanding, we explore here the possibility of combining the EPM with a Polynomial Chaos Expansion (PCE) approach. PCE finds its roots in the pioneering work of Wiener [40], which later inspired the work of Ghanem focused on representing random processes and applications to practical engineering problems, see [41] for a complete overview. For the purpose of efficiently forward propagating the uncertainty, it is possible to build a PCE surrogate of the mapping between some random input of the full computational model (in our case the weights $\boldsymbol{w}_i$ of the barycentric coordinate sampled from the Dirichlet distribution) to a generic output namely, the QoIs $o = o(\boldsymbol{w}_i)$.

The expansion corresponds to the orthogonal projection, into the linear span, of a finite set of orthonormal polynomials $\Psi_k\left(\boldsymbol{w}_i\right)$

$$o(\boldsymbol{w}_i) \doteq \sum_{k=0}^{\infty} c_k \Psi_k\left(\boldsymbol{w}_i\right), \tag{9}$$

where c_k are unknown coefficients and where the index of summation k indicates the polynomial order. In particular, k ranges from 0 to ∞. In practice, an upper arbitrary value P must be set to truncate the expansion. The polynomial basis $\Psi(\boldsymbol{w}_i)$ is chosen such that the

following orthogonality relation, corresponding to the inner product in the L_2 Hilbert space, is satisfied

$$\langle \Psi_i(\boldsymbol{w}_i), \Psi_j(\boldsymbol{w}_i) \rangle = \int \Psi_i(\boldsymbol{w}_i)\Psi_j(\boldsymbol{w}_i)p(\boldsymbol{w}_i)d\boldsymbol{w}_i = \langle \Psi_i(\boldsymbol{w}_i)^2 \rangle \delta_{ij}, \tag{10}$$

and the choice depends on the peculiar distribution characterizing the inputs.

The Dirichlet distribution can be constructed starting from a set of K independent gamma random variables (Γ)

$$Y_1 \sim \Gamma(\alpha_1, \beta), \dots, Y_K \sim \Gamma(\alpha_K, \beta) \tag{11}$$

being α and β the shape and the rate (or scale) parameters, respectively, according to

$$\mathcal{P}_{\text{Dir}}\left(\xi_1, \xi_2; \boldsymbol{\alpha}\right) \sim \left(\frac{Y_1}{V}, \dots, \frac{Y_K}{V}\right), \quad \text{with} \quad V = \sum_{i=1}^{K} Y_i. \tag{12}$$

To reproduce the flat Dirichlet distribution, unit shape and rate parameters were used. In this work we are trying to sample uniformly from a 2-dimensional simplex, therefore we can interpret our problem as dependent on three independent random variables distributed according to the same Γ distribution. According to the Askey scheme, the basis of the PCE surrogate must be Gauss–Laguerre polynomials. With this information, one option is to sample the realizability triangle at the root of Laguerre polynomials and solve a quadrature integration formula to compute the expansion coefficients, see Fig. 1(b). Another possibility is to solve a least square problem minimizing the residual between the surrogate output and the reference data, which is the strategy we adopt here. Once the truncation scheme has been selected, we solve the discrete minimization problem

$$\mathbf{c} = \arg\min_{\mathbf{c}\in\mathbb{R}} \left\{ \frac{1}{N} \sum_{i=1}^{N} \left(o(\boldsymbol{w}_i) - \sum_{k=0}^{P} c_k \Psi_k\left(\boldsymbol{w}_i\right) \right)^2 \right\}, \tag{13}$$

where the $\boldsymbol{w}_i$ is the set of training points (different than the Monte Carlo sample set employed to present the previous analysis). In particular, we decided to rely on a training set of 64 points sampled using the Gauss–Laguerre quadrature rule. Note that this choice is just to differentiate from the random Monte Carlo sampling and to obtain regularly spaced point over the realizability triangle.

Once the expansion coefficients are available, we perform two tests to assess the quality of the surrogate, see [42]. First we evaluate the generalization error

$$\text{Err}_{gen} = \left[\frac{1}{M} \sum_{i=1}^{M} \left(o(\boldsymbol{w}_i) - \sum_{k=0}^{P} c_k \Psi_k\left(\boldsymbol{w}_i\right) \right)^2 \right], \tag{14}$$

considering the data from the Monte Carlo analysis as a validation test set, being M=1000. After, we evaluate the coefficient of determination

$$\text{R}^2 = 1 - \frac{\text{Err}_{gen}}{\text{Var}(\{o(\boldsymbol{w}_1), \dots, o(\boldsymbol{w}_M)\})} \qquad \text{with } \text{R}^2 \in (-\infty, 1], \tag{15}$$

Note that $\text{R}^2 = 1$ indicates a perfect fit.

The error estimators are reported in Figs. 9 and 10, for all the considered values of the angle of attack α. Concerning the Err_{gen}, very small values are obtained throughout the whole range of α, with a general increasing trend towards the upper bound. Nonetheless, the generalization error is well below the acceptable threshold for all the QoIs. The PCEs related to the efficiency generally present the larger error, in the order of $5 \cdot 10^{-2}$, which is by the way acceptable in relation to the absolute values of EF.

The coefficient of determination R^2 is very close to the perfect fit value ($\text{R}^2 = 1$) for all the α, indicating that the surrogate obtained for this test case are of good quality and do not suffer from poor approximation or overfitting issues.

4. Conclusions

Turbulence closures employed in CFD simulations rely on strong inherent model-form assumptions that limit the credibility of numerical predictions for some flow configurations. The direct quantification of epistemic uncertainty is practically intractable and requires the development of advanced UQ techniques. The EPM is designed to efficiently compute uncertainty estimates rather than establish rigorous and provable prediction bounds. In this perspective, the standard EPM provides only a limited analysis of the structural uncertainty affecting the RST. Nonetheless, the question of how these estimates compare with the actual uncertainty is investigated.

In particular, we take advantage of two academic test cases to provide a Monte Carlo analysis concerning the forward propagation of the uncertainty affecting the spectrum of the RST. We stress here that the goal of this paper is not to draw conclusions about the physics of turbulent flows. Indeed, this would require numerical models of large computational cost which would render the Monte Carlo analysis unfeasible. The goal is to expose the implications and limits associated with using the standard EPM w.r.t. adopting a more comprehensive approach. For this reason, we rely on a fixed set up e.g., convergence criteria, grid, numerical scheme, independently of the perturbation applied.

The sampling of the Monte Carlo realizations of the RST is carried out exploiting a flat Dirichlet distribution defined over the realizability space. The data are then post-processed to obtain statistical information concerning the propagation of the turbulence closure epistemic uncertainty to selected quantities of interest. Results confirm that the standard EPM envelope often includes the bulk of the probability density, serving as a rough, yet efficient, criterion for estimating the output uncertainty range. Nonetheless, there exist situations for which a large number of realizations falls outside the standard EPM envelope, or situations for which the standard EPM envelope is overly conservative. These are of utmost relevance for methodologies built on top of the EPM. For instance, in [15], it is stated that design exploration and optimization under turbulence model-form uncertainty was practically never investigated prior to 2020. In this regard, two open research questions are formulated by the Authors. Namely, how to produce reliable uncertainty estimates and how to integrate these into design optimization. In particular, the issues exposed in this work are relevant for both aspects. Indeed, the uncertainty estimates produced by the standard EPM are not always reliable. At the same time, a Monte Carlo-based approach would be too demanding for practical applications that require the evaluation of the output statistics for a large number of iterations e.g., robust design optimization. This is particularly true considering applications of industrial interest for which a Monte Carlo analysis of the turbulence closure structural uncertainty would just be out of question. This latter aspect requires, of course, the implementation of more advanced and efficient UQ techniques.

In this work, the forward uncertainty propagation by means of the construction of PCE surrogates is shown to be a formally viable approach, at least for a test case as simple as a two-dimensional airfoil in a subsonic freestream. Naturally, further investigations should be devoted to improving the efficiency of the process of constructing the surrogate, considering also more complex computational models. In particular, a key aspect is to devise a formal parametrization for the orientation of the RST basis, to efficiently combine it to the eigenvalues perturbation to build PCE surrogates. At the time of writing, Authors suggest different approaches [9,19,21] that may be straightforwardly exploited, but the feasibility of building PCE surrogates for practical applications must be investigated in view of the larger computational cost entailed by the increased dimensionality of the problem.

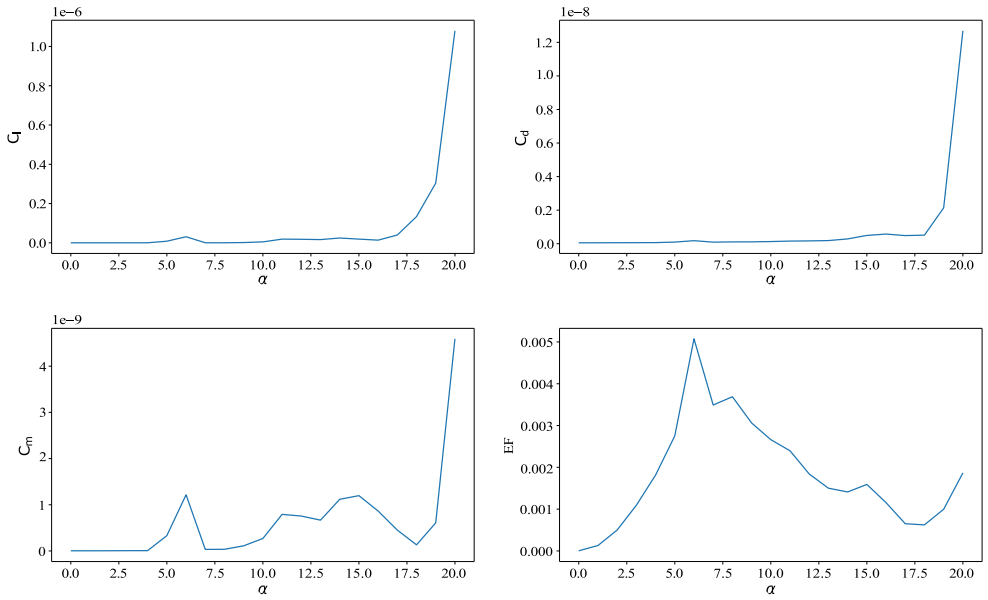

Fig. 9. AIRFOIL. Generalization error (Err_{gen}) of PCE surrogate obtained for the targeted QoIs.

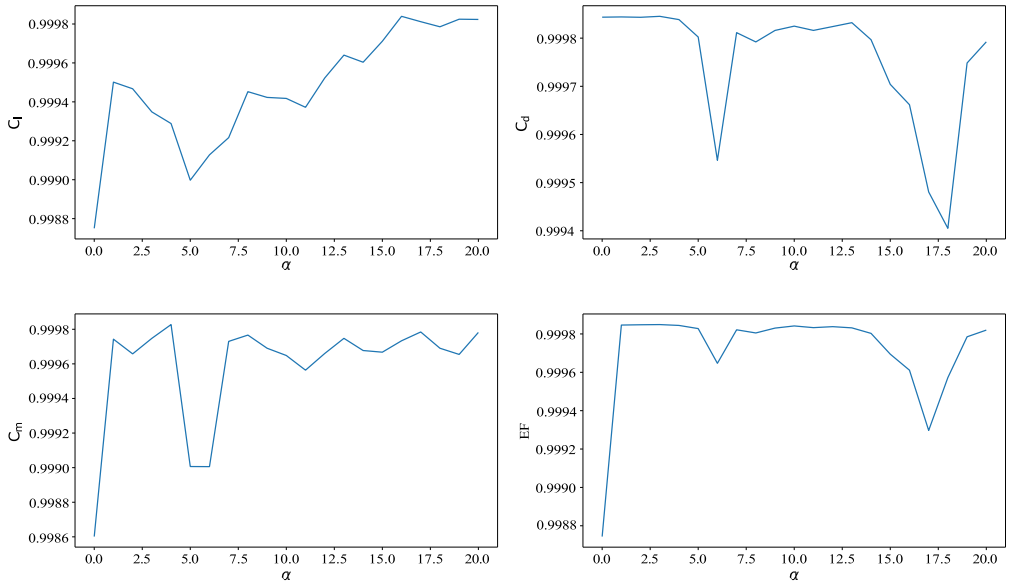

Fig. 10. AIRFOIL. Coefficient of determination (R^2) of PCE surrogate obtained for the targeted QoIs.

Declaration of competing interest

The authors declare the following financial interests/personal relationships which may be considered as potential competing interests: Giulio Gori reports financial support was provided by EU Framework Programme for Research and Innovation Marie Sklodowska-Curie Actions. If there are other authors, they declare that they have no known competing financial interests or personal relationships that could have appeared to influence the work reported in this paper.

Acknowledgments

This work was funded by the European Union (Project 101059320 - UN-BIASED). Views and opinions expressed are, however, those of the author(s) only and do not necessarily reflect those of the European Union or the European Research Executive Agency. Neither the European Union nor the European Research Executive Agency can be held responsible for them.

Data availability

No data was used for the research described in the article.

References

[1] Duraisamy K, Iaccarino G, Xiao H. Turbulence modeling in the age of data. Annu Rev Fluid Mech 2019;51(Volume 51, 2019):357–77. http://dx.doi.org/10.1146/annurev-fluid-010518-040547, URL https://www.annualreviews.org/content/journals/10.1146/annurev-fluid-010518-040547.

[2] Wu J, Xiao H, Sun R, Wang Q. Reynolds-averaged Navier–Stokes equations with explicit data-driven Reynolds stress closure can be ill-conditioned. J Fluid Mech 2019;869:553–86. http://dx.doi.org/10.1017/jfm.2019.205.

[3] Brener BP, Cruz MA, Thompson RL, Anjos RP. Conditioning and accurate solutions of Reynolds average Navier–Stokes equations with data-driven turbulence closures. J Fluid Mech 2021;915:A110. http://dx.doi.org/10.1017/jfm.2021.148.

[4] Shan X, Cao W, Zhang W. New interpretation for error propagation of data-driven Reynolds stress closures via global stability analysis. Phys Fluids 2025;37(2):025217.

[5] Xiao H, Cinnella P. Quantification of model uncertainty in RANS simulations: A review. Prog Aerosp Sci 2019;108:1–31. http://dx.doi.org/10.1016/j.paerosci.2018.10.001, URL https://www.sciencedirect.com/science/article/pii/S0376042118300952.

[6] Emory M, Pecnik R, Iaccarino G. Modeling structural uncertainties in Reynolds-averaged computations of shock/boundary layer interactions. 2011, http://dx.doi.org/10.2514/6.2011-479, AIAA 2011-479, arXiv:https://arc.aiaa.org/doi/pdf/10.2514/6.2011-479.

[7] Emory M, Larsson J, Iaccarino G. Modeling of structural uncertainties in Reynolds-averaged Navier-Stokes closures. Phys Fluids 2013;25(11):110822. http://dx.doi.org/10.1063/1.4824659, arXiv:https://pubs.aip.org/aip/pof/article-pdf/doi/10.1063/1.4824659/13379908/110822_1_online.pdf.

[8] Matha M, Morsbach C. Improved self-consistency of the Reynolds stress tensor eigenspace perturbation for uncertainty quantification. Phys Fluids 2023;35(6):065130. http://dx.doi.org/10.1063/5.0149747.

[9] Iaccarino G, Mishra AA, Ghili S. Eigenspace perturbations for uncertainty estimation of single-point turbulence closures. Phys Rev Fluids 2017;2:024605. http://dx.doi.org/10.1103/PhysRevFluids.2.024605, URL https://link.aps.org/doi/10.1103/PhysRevFluids.2.024605.

[10] Jofre L, Domino S, Iaccarino G. A framework for characterizing structural uncertainty in large-eddy simulation closures. Flow Turbul Combust 2018;100:341–63.

[11] Mishra AA, Iaccarino G. Theoretical analysis of tensor perturbations for uncertainty quantification of Reynolds averaged and subgrid scale closures. Phys Fluids 2019;31(7):075101. http://dx.doi.org/10.1063/1.5099176.

[12] Xiao H, Wu J, Wang J, Sun R, Roy CJ. Quantifying and reducing model-form uncertainties in Reynolds-averaged Navier–Stokes simulations: A data-driven, physics-informed Bayesian approach. J Comput Phys 2016;324:115–36. http://dx.doi.org/10.1016/j.jcp.2016.07.038.

[13] Razaaly N, Gori G, Iaccarino G, Congedo PM. Optimization of an ORC supersonic nozzle under epistemic uncertainties due to turbulence models. In: GPPS 2019 - global power and propulsion society. Zurich, Switzerland; 2019, URL https://hal.inria.fr/hal-01982227.

[14] Cook L, Mishra A, Jarrett J, Willcox K, Iaccarino G. Optimization under turbulence model uncertainty for aerospace design. Phys Fluids 2019;31:105111. http://dx.doi.org/10.1063/1.5118785.

[15] Mishra AA, Mukhopadhaya J, Alonso J, Iaccarino G. Design exploration and optimization under uncertainty. Phys Fluids 2020;32(8):085106. http://dx.doi.org/10.1063/5.0020858.

[16] Li A, Wang T, Chen J, Huang Z, Xi G. Adjoint design optimization under the uncertainty quantification of Reynolds-averaged Navier-Stokes turbulence model. AIAA J 2024;1–12. http://dx.doi.org/10.2514/1.J063643, 0.

[17] Gori G, Congedo PM, Le Maître O. A confidence-based aerospace design approach robust to structural turbulence closure uncertainty. Comput & Fluids 2022;246:105614. http://dx.doi.org/10.1016/j.compfluid.2022.105614.

[18] Huang Z, Mishra AA, Iaccarino G. A Nonuniform Perturbation to Quantify RANS Model Uncertainties. Stanford, CA: Center for Turbulence Research Annual Research Briefs, Stanford Univ.; 2020, p. 223–32.

[19] Xiao H, Wang J-X, Ghanem RG. A random matrix approach for quantifying model-form uncertainties in turbulence modeling. Comput Methods Appl Mech Engrg 2017;313:941–65. http://dx.doi.org/10.1016/j.cma.2016.10.025, URL https://www.sciencedirect.com/science/article/pii/S0045782516313822.

[20] Wang J-X, Sun R, Xiao H. Quantification of uncertainties in turbulence modeling: A comparison of physics-based and random matrix theoretic approaches. Int J Heat Fluid Flow 2016;62:577–92. http://dx.doi.org/10.1016/j.ijheatfluidflow.2016.07.005, URL https://www.sciencedirect.com/science/article/pii/S0142727X16300339.

[21] Wu J-L, Xiao H, Paterson E. Physics-informed machine learning approach for augmenting turbulence models: A comprehensive framework. Phys Rev Fluids 2018;3:074602. http://dx.doi.org/10.1103/PhysRevFluids.3.074602.

[22] Wu J-L, Sun R, Laizet S, Xiao H. Representation of stress tensor perturbations with application in machine-learning-assisted turbulence modeling. Comput Methods Appl Mech Engrg 2019;346:707–26. http://dx.doi.org/10.1016/j.cma.2018.09.010.

[23] Jewell E, Farhat C, Soize C. A tractable nonparametric probabilistic approach for modeling and quantifying model-form uncertainty in turbulent CFD. J Comput Phys 2025;536:114067. http://dx.doi.org/10.1016/j.jcp.2025.114067, URL https://www.sciencedirect.com/science/article/pii/S002199912500350X.

[24] Palacios F, Alonso JJ, Duraisamy K, Colonno M, Hicken J, Aranake A, Campos A, Copeland S, Economon TD, Lonkar A, Lukaczyk T, Taylor T. Stanford university unstructured (SU^2): An open-source integrated computational environment for multi-physics simulation and design. 2013, http://dx.doi.org/10.2514/6.2013-287, AIAA 2013-287, arXiv:https://arc.aiaa.org/doi/pdf/10.2514/6.2013-287.

[25] Economon TD, Mudigere D, Bansal G, Heinecke A, Palacios F, Park J, Smelyanskiy M, Alonso JJ, Dubey P. Performance optimizations for scalable implicit RANS calculations with SU2. Comput & Fluids 2016;129:146–58. http://dx.doi.org/10.1016/j.compfluid.2016.02.003, URL https://www.sciencedirect.com/science/article/pii/S0045793016300214.

[26] Mishra AA, Mukhopadhaya J, Iaccarino G, Alonso J. Uncertainty estimation module for turbulence model predictions in SU2. AIAA J 2019;57(3):1066–77. http://dx.doi.org/10.2514/1.J057187.

[27] Pope SB. Turbulent Flows. Cambridge University Press; 2000.

[28] Gorlé C, Iaccarino G. A framework for epistemic uncertainty quantification of turbulent scalar flux models for Reynolds-averaged Navier-Stokes simulations. Phys Fluids 2013;25(5):055105. http://dx.doi.org/10.1063/1.4807067, arXiv:https://doi.org/10.1063/1.4807067.

[29] Simonsen AJ, Krogstad PÅ. Turbulent stress invariant analysis: Clarification of existing terminology. Phys Fluids 2005;17(8):088103. http://dx.doi.org/10.1063/1.2009008, arXiv:https://doi.org/10.1063/1.2009008.

[30] Schumann U. Realizability of Reynolds-stress turbulence models. Phys Fluids 1977;20(5):721–5. http://dx.doi.org/10.1063/1.861942, arXiv:https://aip.scitation.org/doi/pdf/10.1063/1.861942.

[31] NASA langley turbulence modeling resource website. 2019, http://turbmodels.larc.nasa.gov, (Accessed 11 November 2019).

[32] Jespersen DC, H. T, Childs ML. OVERFLOW: Turbulence Modeling Resource Validation Results. (Tech. rep., NASA-2016-01). NASA Ames Research Center, Moffett Field, CA; 2010.

[33] Driver DM, Seegmiller HL. Features of a reattaching turbulent shear layer in divergent channelflow. AIAA J 1985;23(2):163–71. http://dx.doi.org/10.2514/3.8890.

[34] Eça L, Hoekstra M, Roache P. Verification of calculations: an overview of the lisbon workshop. 2005, http://dx.doi.org/10.2514/6.2005-4728, AIAA 2005-4728.

[35] Eça L, Hoekstra M, Roache P. Verification of calculations: An overview of the 2nd lisbon workshop. In: 18th AIAA computational fluid dynamics conference. http://dx.doi.org/10.2514/6.2007-4089.

[36] Eça L, Hoekstra M, Roache P, Coleman H. Code verification, solution verification and validation: An overview of the 3rd lisbon workshop. In: 19th AIAA computational fluid dynamics. http://dx.doi.org/10.2514/6.2009-3647.

[37] Menter FR. Zonal two equation k-w turbulence models for aerodynamic flows. In: AIAA 1993-2906. 23rd fluid dynamics, plasmadynamics, and lasers conference. 1993, http://dx.doi.org/10.2514/6.1993-2906.

[38] van Leer B. Towards the ultimate conservative difference scheme. V. A second-order sequel to godunov's method. J Comput Phys 1979;32(1):101–36. http://dx.doi.org/10.1016/0021-9991(79)90145-1, URL https://www.sciencedirect.com/science/article/pii/0021999179901451.

[39] Gori G, Congedo PM, Le Maître O. On the sensitivity of structural turbulence uncertainty estimates to time and space resolution. Comput & Fluids 2021;229:105081. http://dx.doi.org/10.1016/j.compfluid.2021.105081, URL https://www.sciencedirect.com/science/article/pii/S0045793021002401.

[40] Wiener N. The homogeneous chaos. Amer J Math 1938;60(4):897–936, URL http://www.jstor.org/stable/2371268.

[41] Ghanem RG, Spanos PD. Stochastic finite elements: a spectral approach. Berlin, Heidelberg: Springer-Verlag; 1991.

[42] Sudret B. Polynomial chaos expansions and stochastic finite element methods. In: Kok-Kwang Phoon JC, editor. risk and reliability in geotechnical engineering. CRC Press; 2015, p. 265–300, URL https://hal.science/hal-01449883.